

CONCERNING THE FERMI SURFACE OF ALUMINUM

V. P. NABEREZHNYKH and V. P. TOLSTOLUZHSKIĬ

Physico-technical Institute of Low Temperatures, Academy of Sciences, Ukrainian S.S.R.

Submitted to JETP editor May 22, 1963

J. Exptl. Theoret. Phys. (U.S.S.R.) 46, 18-27 (January, 1964)

The effective-mass anisotropy of majority current carriers in aluminum is derived from a study of cyclotron resonance in the three principal crystallographic planes. By comparing the experimental results with calculations performed on an electronic computer for the nearly-free-electron model it was possible to indicate the electron orbits for almost all experimentally observed effective masses and to demonstrate their good agreement with the chosen Fermi surface model. The anisotropy of experimental cross-section areas measurable from the de Haas-van Alphen effect was also calculated.

INTRODUCTION

A detailed study of the anisotropy of small effective masses in aluminum [1] has shown that Harrison's model of the Fermi surface for the third zone provides a fairly adequate interpretation of experimental observations. Still better agreement of the model with experiment can be expected for the Fermi surface in the second zone, which is shown in Fig. 1, where the lattice potential should have a smaller influence.

Galkin et al. [2] have attempted to interpret qualitatively the anisotropy of large effective masses in aluminum for the (001) plane using Harrison's model for the Fermi hole surface in the second zone. However, the complexity of the resonance spectra and the geometry of the model itself in some instances prevented a unique identification of resonance orbits. The effective mass  $\sim 0.8 m_0$  was incorrectly interpreted as the mass in the central section.

In order to obtain a more reliable interpretation of the experimental effective masses we have performed a detailed calculation of all possible resonance orbits on the model of "nearly free electrons," using an M-20 electronic computer. We thus derived the dependence of the effective masses  $m^*$  and cross-section areas  $S$  on  $k_H$  for all directions of the magnetic field  $H$  in the three principal crystallographic planes (001), (110), and (111).

The effective mass was defined as the sum of all angles at which orbital segments are visible from the corresponding centers, divided by  $2\pi$ . This definition of the effective mass [3] is based on the fact that if the Fermi surface is repre-

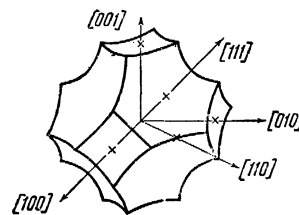


FIG. 1. Model of Fermi surface in the second zone (a pocket of holes) of aluminum.

sented as a sphere intersected by Bragg planes, then under the influence of a magnetic field the projection of an electron on the plane  $k_H = \text{const}$  will move with constant angular velocity, performing finite jumps at intersections of the orbit with the Bragg planes. If it is assumed that the mass associated with the sphere in the absence of Bragg reflections is  $m_0$ , then the sum of all angles at which orbital segments are visible, divided by  $2\pi$ , gives the effective mass in units of  $m_0$ .

This definition of the effective mass can be applied to the case of a reduced zone. Since in this case the orbit consists of segments which are circular arcs, the effective mass in a given cross section can be determined if we know the angles at which these orbits are visible from the centers of the respective circles.

Our problem was formulated as follows. Since aluminum has a face-centered cubic lattice, it has a body-centered cubic reciprocal lattice with the edge length  $2(2\pi/a)$ ,  $a$  being the lattice constant. Free-electron spheres are centered on the vertices of the cube and on the centers of neighboring cubes (for the second zone). The radius of each of these 14 spheres for aluminum is

$$R_F = (3\pi^2 n/a^3)^{1/3} \approx 1.128 (2\pi/a).$$

Here  $n$  is the number of electrons in the unit cell; for aluminum  $n = 12$  because each unit cell of the trivalent metal contains four atoms.

In order to determine the required orbital parameters we found the intersection points of the circles lying in the plane  $k_H = \text{const}$ . For this purpose the computer solved simultaneously the equations of the spheres and of the planes  $k_H = \text{const}$ . The parameter  $k_H$  was varied in steps of  $0.01 \times (2\pi/a)$  up to values for which multiply connected regions began to appear in the cross section. No simple and reliable algorithm could be found for large  $k_H$ .

For the resultant polygonal figure in the plane  $k_H = \text{const}$  the area and effective mass were determined as functions of  $k_H$  for a given direction of  $H$ . The angle  $\theta$  defining the direction of  $H$  at which the calculation was performed was varied in  $2.5^\circ$  steps, thus covering, when symmetry is taken into account, the entire required angular region for the given crystallographic plane.

Since the calculated dependence of the effective mass on  $k_H$  varied greatly as the angle  $\theta$  was changed, it was desirable to estimate the magnitude of resonance for the different orbits. The amplitude and width of resonance, all other conditions remaining identical, are determined by the

sharpness of the effective-mass extremum, i.e., by the rate at which  $m^*$  changes with  $k_H$ . At the extremum we have

$$m^*(k_H) = m^*(k_H^0) + (\Delta k_H)^2 \partial^2 m^*(k_H) / \partial k_H^2,$$

where  $k_H^0$  is the value of  $k_H$  at which the extremum of  $m^*$  is reached. The quantity

$$\frac{\partial^2 m^*(k_H)}{\partial k_H^2} \frac{1}{m^*(k_H^0)} = \frac{\Delta m^*(k_H)}{m^*(k_H)} \frac{1}{(\Delta k_H)^2}$$

will characterize the possible resonance intensity, since the sharper the extremum, the smaller the number of conduction electrons contributing to the resonance. Since  $\Delta k_H$  was everywhere identical, the characteristic of resonance was taken to be  $\Delta m^*/m^*$  corresponding to the interval  $\Delta k_H$ .

Another important characteristic of the resonance orbits is the mean drift velocity per period of electrons along a magnetic field  $H$ :

$$\bar{v}_H = (\hbar/2\pi m^*) \partial S(k_H) / \partial k_H.$$

The calculation showed that the areal extremum does not, as a rule, coincide with the mass extremum (except for orbits with  $k_H = 0$ ). Therefore a knowledge of  $\bar{v}_H$  is essential for a comparison with experiment. When a sample has a "bad" surface and  $H$  is somewhat inclined to the surface, resonance in orbits with high drift ve-

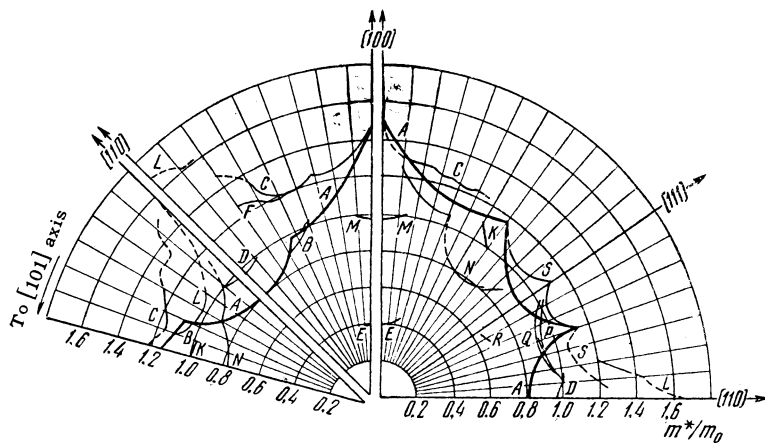


FIG. 2. Calculated angular dependences of extremal effective masses for Fermi surface (of pocket of holes) of aluminum in the three crystallographic planes (110), (001), and (111). Heavy lines—effective mass in the central section; dashed lines—effective masses with low probability of resonance; letters denote resonances in different orbits.

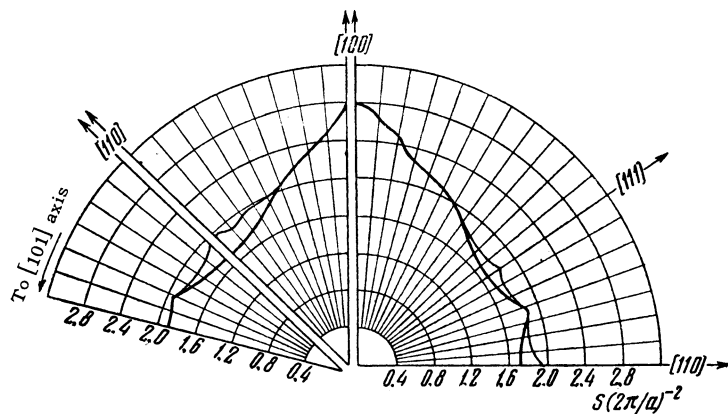


FIG. 3. Calculated angular dependences of extremal cross-sectional areas for Fermi surface (of pocket of holes) of aluminum in the three crystallographic planes (110), (001), and (111). Heavy curves—areas of central sections.

locity will be strongly reduced (electrons move quickly into the interior of the metal) or even disappear.

Since the computer derived discrete values of the function  $S(k_H)$  at intervals  $\Delta k_H$ ,  $\bar{v}_H$  was computed as  $(\hbar/2\pi m^*)\Delta S/\Delta k_H$  for  $k_H^0$ , where the effective mass either had an extremum or varied only slightly with changes of  $k_H$ .

Figures 2 and 3 show the calculated angular dependences of effective masses and cross-section areas for the three planes (110), (001), and (111) (from right to left). The experimental data and calculations will now be considered separately for each plane.

**EXPERIMENTAL DATA AND THEIR INTERPRETATION**

(001) plane. We shall first consider briefly the behavior of the effective masses in the nearly-free-electron model. Figure 4 represents the calculated dependence of the masses on  $k_H$  for certain directions of  $H$ . For  $\theta = 0^\circ$ , which is the case of  $H \parallel [100]$ , the effective mass, viewed rigorously, has an extremum only in the central section. However, for  $k_H = 0.47 k_0$  and  $0.9 k_0$ , although the derivative  $\partial m^*/\partial k_H$  does not vanish, the variation of the mass is so slight that the probability of a very sharp resonance is great. When it is also considered that under the influence of the lattice potential sharp corners of the Fermi surface must be rounded off, an extremum of the mass can also be expected on these orbits.

It is interesting that the effective mass in the central section at  $\theta = 0^\circ$  is maximal, but that with a small departure of  $H$  from this direction it becomes minimal. The separation of the extrema increases gradually with the angle  $\theta$ , and the corresponding masses differ greatly. An increase of  $\theta$  also impairs the conditions for realizing resonance in the cases of orbits E and M at  $k_H \sim 0.9 k_0$  and  $\sim 0.47 k_0$ , respectively.

A very distinctive mass distribution arises when  $\theta = 25^\circ$ . At this angle the mass again becomes maximal for  $k_H = 0$ , and minimal for  $k_H = 0.15 k_0$ . In addition, on a large broad maximum the mass can exhibit both a minimum and a maximum. It is then not at all clear whether resonance can be resolved on these orbits or will be observed as a single broad line. Jumps of the mass, which are observed in the region  $k_H \sim 0.65 k_0$ , evidently do not yield a perceptible resonance because of their sharpness.

With further variation of  $\theta$  the mass minimum B for  $k_H \sim 0.15 k_0$  again disappears; at  $k_H = 0$

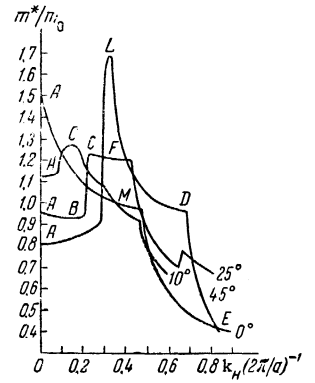


FIG. 4. Effective mass as a function of  $k_H$  for certain directions of the magnetic field  $H$  in the (001) plane. The angle between  $H$  and  $[100]$  axis is denoted at the end of each curve; the letters denote the extrema corresponding to the effective masses in Fig. 2.

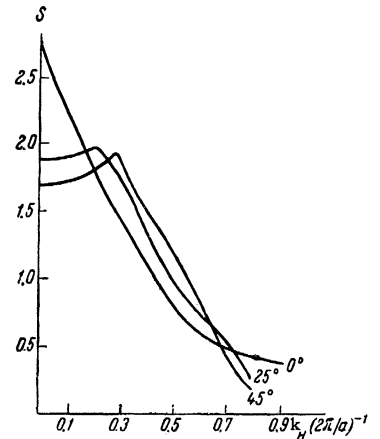


FIG. 5. Cross-section area as a function of  $k_H$  for certain directions of  $H$  in the (001) plane. The angle between  $H$  and the  $[100]$  axis is denoted at the end of each curve.

minimum is again reached. The broad maximum for  $k_H \sim 0.3 k_0$  is greatly narrowed and at  $k_H \sim 0.65 k_0$  resonance again becomes possible.

For the cross-section areas, whose dependence on  $k_H$  is shown in Fig. 5, the number of extrema is considerably smaller. At  $\theta = 0^\circ$  an extremum (maximum) of  $S(k_H)$  is reached only when  $k_H = 0$ . With increasing  $\theta$  the areal maximum shifts towards larger  $k_H$ ;  $S(k_H)$  has a minimum at  $k_H = 0^\circ$ .

The value of  $k_H$  at which a maximum of  $S(k_H)$  occurs coincides with the value of  $k_H$  where the change of the effective mass is practically discontinuous.

Figure 6 shows the experimental anisotropy of effective masses in the (001) plane. All masses are seen to be much larger than the calculated values. Therefore the orbits can be identified only from the anisotropy and amplitude estimates.

When  $H$  is parallel to a fourfold axis only two resonances are observed experimentally, with effective masses  $m_1^* \approx 0.7 m_0$  and  $m_2^* \approx 1.43 m_0$ . These resonances are observed in a very limited angle interval; the mass ratio  $m_2^*/m_1^*$  is approximately the same as for the calculated masses E and M. We can thus identify orbits associated with the indicated experimental masses, and the orbits E and M occurring with  $k_H = 0.9 k_0$  and  $0.47 k_0$ .

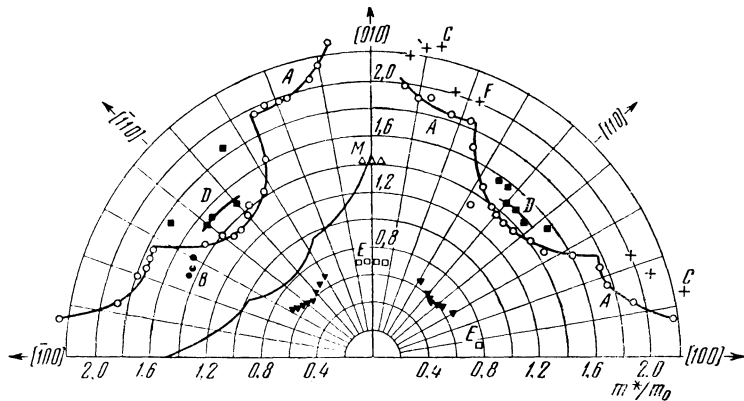


FIG. 6. Experimental anisotropy of effective masses in (001) plane. Line without experimental points—calculated mass anisotropy in central section. The letter symbols are the same as in Fig. 2.

The calculations show that for these orbits when  $\theta > 7.5^\circ$ ,  $\Delta m^*/m^*$  becomes very large and the orbits can hardly be observed at much larger angles.

The fact that in this direction a third resonance A in the central section is not observed can be accounted for by the result that for the orbit A the relative change of mass  $\Delta m^*/m^*$  is almost one order greater than for E and M. It is interesting to note that in the given field direction the de Haas-van Alphen oscillations could not be observed in extremely high fields, although these oscillations were pronounced in other directions. [4]

When the field forms an angle of about  $7.5^\circ$  with the axis two additional resonances appear with  $m^* \sim 2.0 m_0$  and  $\sim 2.2 m_0$  (designated in Figs. 6 and 8 by circles and crosses, respectively). The first of these resonances is observed steadily near all fourfold axes with an amplitude that increases with  $\theta$ ; the second resonance, which is weaker, is reproduced poorly for similar directions of H. Since the surface of the sample was not smoothed out for each angle  $\theta$  separately, it is suggested that this resonance occurs in an orbit with an appreciable drift velocity  $\bar{v}_H$ , and that its poor reproducibility is associated with the changing field angle as the sample is rotated.

The behavior of these resonances leads to their identification with the calculated resonances A and C, which correspond to orbits in the central section with maximal mass. Indeed, in complete agreement with experiment resonance A should grow in intensity with  $\theta$  up to  $\sim 25^\circ$ , while the effective mass is considerably diminished. Resonance C occurs on orbits with  $\bar{v}_H \approx 0.6 \times 10^8$  cm/sec and its observation may be difficult.

At  $\theta = 25^\circ$  from the  $[100]$  axis an easily observed resonance B occurs in addition to A. This resonance splitting is characteristically absent for the same angle from other fourfold axes, thus indicating that the plane of the sample deviates from the (001) plane.

The splitting can be accounted for completely by considering the dependence of the mass on  $k_H$  (Fig. 4). At  $\theta = 25^\circ$ , in addition to the extremum at  $k_H = 0$ , a minimum occurs at  $k_H = 0.14 k_0$ , at which the mass is somewhat smaller than the mass A. The calculation also shows that for resonance B,  $\Delta m^*/m^*$  is considerably smaller than for A. This situation is also accompanied by a small drift velocity  $\bar{v}_H \approx 0.04 \times 10^8$  cm/sec. The mass difference, which is small (0.97 and  $0.94 m_0$ ) for exact orientation, can be considerably increased when the sample is inclined in one direction, and decreased for the opposite direction. In this case resonances A and B can be resolved for identical field directions while they are unresolved for other similar directions, even without taking into account that orbital parameters may vary at the same time.

With regard to resonance F corresponding to a minimum of  $m^*$  at  $k_H = 0.39 k_0$ , which should also be observed at  $\theta = 25^\circ$ , it is not clear, as already mentioned, whether this could be observed separately from resonance C or whether the two resonances cannot be resolved. Since the effective-mass difference between C and F is about 4%, the relative width  $\Delta H/H > 5\%$  of the observed lines suggests that these resonances cannot be resolved. However, considering that the parameters of orbit F are considerably better than those of C the oscillation period is most probably determined by the mass F.

As  $\theta$  continues to increase, the effective mass corresponding to resonance A begins to decrease sharply, as should occur for a mass in the central section; the resonance amplitude, which is weak at  $\theta = 30^\circ$ , gradually increases to a maximum at  $45^\circ$ . It should be noted, however, that although the amplitude grows, it remains smaller than at  $\theta \sim 15-20^\circ$ , although  $\Delta m^*/m^*$  should remain approximately unchanged according to the calculation.

FIG. 7. Experimental anisotropy of effective masses in the (110) plane. The letter symbols are the same as in Fig. 2.

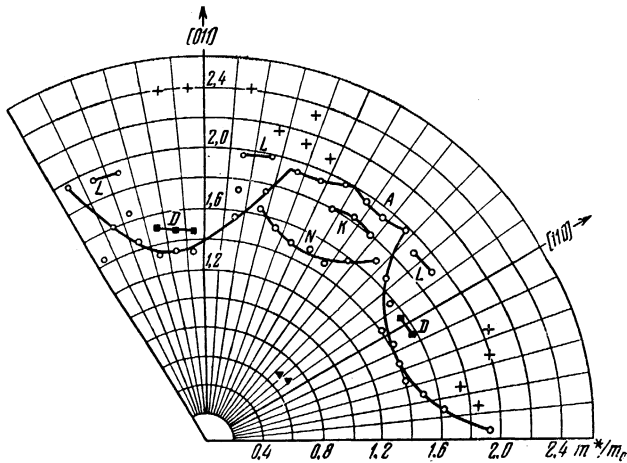
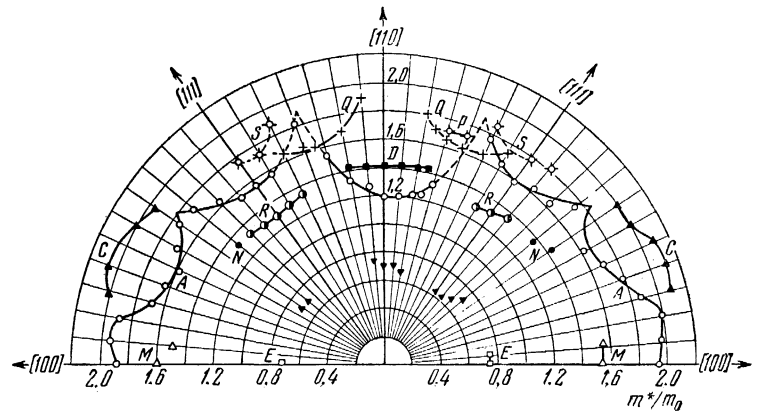


FIG. 8. Experimental anisotropy of effective masses in the (111) plane. The letter symbols are the same as in Fig. 2.

At  $\theta$  close to  $45^\circ$  three effective masses are observed experimentally. The Harrison model furnishes a good interpretation of two of these, while the third does not follow from the calculation. At  $\theta = 45^\circ$  the calculation actually gives three masses: A, L; and D corresponding to  $k_H = 0$ ,  $0.33 k_0$ , and  $0.69 k_0$ . Here mass D is somewhat larger than A, and the resonance conditions for the former can be impaired both by a large value  $\bar{v}_H \sim 10^8$  cm/sec and by  $\Delta m^*/m^* \approx (1-3) \times 10^{-3}$ . Mass L should be almost twice as large, and may be unobservable because of the very sharp maximum ( $\Delta m^*/m^* \sim 2 \times 10^{-2}$ ).

Masses smaller than that in the central section are not obtained by calculation, but experiment yields  $\sim 0.6 m_0$ , while the mass in the central section is  $\sim 1.3 m_0$ . This result suggests that the mass  $\sim 0.6 m_0$  pertains to orbits not lying on a large Fermi surface. Since the resonance corresponding to this mass is very broad and not sharply defined, it may represent a logarithmic resonance for values of  $k_0$  associated with multiply connected regions.

(110) plane. In this plane the behavior of the calculated effective masses differs somewhat from their behavior in the (001) plane. For example, the mass extremum in the central section also splits with a deviation from the [100] axis, but the splitting results in three, rather than two, extrema. The extremum for  $k_H = 0$  is a maximum up to  $\theta = 35^\circ$ , while  $\Delta m^*/m^*$  decreases as  $\theta$  increases, reaching a minimum at  $\theta = 25^\circ$ . At  $35^\circ$ ,  $\Delta m^*/m^*$  again becomes large, but remains smaller than at  $\theta = 0^\circ$ .

Another resolved mass maximum, denoted in the figures by C, is very sharp, with some broadening in the range  $\theta = 15-25^\circ$ .

The mass minimum N, which lies between the first two maxima, also is accompanied by a large value of  $\Delta m^*/m^*$ , which decreases as  $\theta$  increases. At  $\theta = 35^\circ$  it becomes smaller than for all other extrema in this section.

The calculated mass distribution presents a very complex picture in the range  $\theta = 57.5-80^\circ$ . Here the extrema A and S are accompanied by two additional extrema P and Q. In the range  $\theta = 65-75^\circ$  the value of  $\Delta m^*/m^*$  for the latter becomes considerably smaller than for the extrema A in the central section. At  $\theta = 90^\circ$ , i.e. for  $H \parallel [110]$ , the mass distribution is, of course, the same as that already described in the (001) plane at  $\theta = 45^\circ$ .

Let us now consider the behavior of the experimental effective masses shown in Fig. 7. For H along fourfold axes, as in the (001) plane, the observed resonances give the effective masses E and M. At  $\theta > 7.5^\circ$  from the [100] axis, resonances E and M disappear, in complete agreement with the calculation. Moreover, in this direction the mass A is observed, while its anisotropy around the fourfold axis differs from the calculation. This can be understood from the very strong anisotropy of this mass and the deviation

of the sample's surface from the crystallographic plane. Indeed, if the plane of the sample is somewhat inclined toward a fourfold axis, then  $H$  can never be parallel to this axis, near which the mass will then be isotropic.

For  $\theta = 15-35^\circ$  resonances with the two masses A and C are again observed experimentally. The anisotropy in this angular range of A, which we have assigned to the central section, agrees fully with the calculation. Mass C must evidently be assigned to a mass maximum in the region  $k_H \sim 0.2-0.5 k_0$ . For some reason a resonance corresponding to mass N is not observed in this range of  $\theta$ , although the corresponding calculated value of  $\Delta m^*/m^*$  is somewhat smaller than for C. The resonance corresponding to this mass occurs only in the region  $\theta = 35-40^\circ$ , where  $\Delta m^*/m^*$  becomes minimal. However, the observed resonances N differ somewhat in intensity for [100] and  $[\bar{1}00]$  at  $\theta = 35^\circ$ . In the first case resonance N is stronger, while in the second case the resonance A is stronger, although resonance N should be maximal in both cases. This difference appears to result from inaccurate orientation of the sample. The general picture given by the calculation is similar to that observed at  $\theta = 35-40^\circ$  from the [100] axis for exact orientation.

At the given angles the mass maximum in the central section becomes very sharp, whereas the minimum N for  $k_H = 0.51 k_0$  becomes very broad and resonance with this mass should be maximal. Inexact orientation can, of course, affect this situation. With further increase of  $\theta$ , resonance A increases in intensity while the corresponding mass diminishes, in full agreement with the calculation for the orbit in the central section.

At  $\theta \approx 50-80^\circ$  experiment reveals some resonances which should evidently be identified with the calculated effective masses A, P, Q, and S. Since the experimental points were obtained  $5^\circ$  apart and in a narrow angular interval we observe several close masses differing in anisotropy, a given point cannot always be assigned uniquely to a particular orbit. However, in the given range of  $\theta$  the observed picture resembles the calculated anisotropy in general. Mass R is an exception. Although at  $\theta \approx 55^\circ$  the calculation gives a mass smaller than in the central section, this corresponds to a smooth change of  $m^*$  as a function of  $k_H$  near values of  $k_H$  associated with multiply connected regions (as for masses E and M) and large values of  $\Delta m^*/m^*$ . It remains possible that when the Fermi surface is somewhat deformed around sharp corners such orbits will

exhibit a smoother dependence of  $m^*$  on  $k_H$  and resonance can occur.

As  $H$  approaches the [110] axis the observed resonance pattern becomes similar to that observed in the (001) plane. Here also two masses A and D are observed, which are confirmed by the calculation.

In addition to the effective masses already considered, in the (110) plane masses  $\sim 0.7 m_0$  are observed at  $\theta \approx 90^\circ$  and  $40^\circ$ . As in the case of the (001) plane, the calculation does not indicate the existence of these masses for a large Fermi surface.

(111) plane. For  $H \parallel [110]$  the calculated effective-mass distribution in this plane is the same as in the two other planes. When  $H$  deviates from this direction the mass in the central section must increase, while the mass L corresponding to a large mass maximum for  $k_H \approx 0.33 k_0$  decreases sharply, with  $\Delta m^*/m^*$  having considerable magnitude up to  $\theta = 10^\circ$ . As in the (001) and (110) planes, the effective mass D can be observed in a very limited angular range ( $\theta \pm 5^\circ$ ). Also, at  $\theta > 2.5^\circ$  two mass extrema C and N appear, for  $k_H = 0.32$  and  $0.34 k_0$ , respectively.

The minimal mass N is associated with an appreciable value of  $\Delta m^*/m^*$ , which decreases as  $\theta$  increases and at  $\theta = 13-15^\circ$  becomes the same as in the central section. For mass C,  $\Delta m^*/m^*$  also decreases as  $\theta$  increases, becoming very small at  $\theta = 25-20^\circ$ . Near  $k_H = 0$  at  $\theta = 20^\circ$  an additional minimum mass B appears with small  $\Delta m^*/m^*$ , but disappears at  $\theta = 25^\circ$ . In the range  $\theta = 25-30^\circ$  we find a mass K corresponding to a value of  $k_H$  near which multiply connected regions arise.

Let us now consider the experimental anisotropy of effective masses represented in Fig. 8. Here we observe some departure from the 30-degree symmetry; this is accounted for by the  $5-6^\circ$  deviation of the sample's surface from the (111) plane. Nevertheless, the angular dependences of the effective masses are in good agreement with the calculation for an exact orientation.

For  $H$  oriented close to the [110] axis we observe, as expected, a resonance A corresponding to an orbit in the central section and a resonance with a somewhat larger mass (denoted in Fig. 8 by black squares), which apparently corresponds to mass D. The mass anisotropy of resonance A in this angular range agrees very well with the calculation. For  $\theta \approx 7.5-12.5^\circ$  resonance is observed with mass  $\sim 1.95 m_0$ , which in all probability corresponds to the calculated resonance L.

In the range  $\theta \approx 20-30^\circ$  we observe, in addi-

tion to the resonance A corresponding to the central section, two additional resonances with smaller effective masses. The anisotropy of the smallest mass is very similar to the anisotropy of the calculated mass N, although it is not entirely clear why the corresponding resonance is not observed at  $\theta \approx 15^\circ$ , where  $\Delta m^*/m^*$  becomes still smaller than at  $\theta = 30^\circ$ . This may possibly be associated with a considerably larger drift velocity along H, which at  $\theta = 15^\circ$  is  $\approx 0.2 \times 10^8$  cm/sec, while at  $\theta \approx 30^\circ$  we have  $\bar{v}_H \approx 0.07 \times 10^8$  cm/sec.

The resonance with the mass  $\sim 1.8 m_0$  must evidently be identified with the calculated resonance K. In addition to the described resonances, certain other resonances are observed with the corresponding masses denoted in Fig. 7 by crosses. These resonances are reproduced poorly along similar directions of H, possibly as a result of a high drift velocity along H, and evidently belong to resonances C.

### CONCLUSION

The foregoing comparison between the experimental angular dependences of large effective masses in three crystallographic planes and similar calculations based on the nearly-free-electron model has shown their good qualitative agreement. Most of the experimentally observed effective masses can be identified with the calculated masses and the values of  $k_H$  for the resonance orbits can be given. The good agreement of the results not only for orbits with  $k_H = 0$  but also for other orbits where a mass extremum is reached, represents strong confirmation of many topological properties of the Fermi surface. Cyclotron resonance can thus sometimes furnish much more information than the deHaas-van Alphen effect, for example. When we compare the aniso-

tropy of calculated effective masses with the calculated anisotropy of extremal cross sectional areas it becomes clear that the topological properties are much more pronounced and significant in connection with the former. This significance appears both in the mass anisotropy and in the large number of resonance orbits.

The agreement with Harrison's model of the Fermi surface is only qualitative; the quantitative results differ considerably. All the experimental effective masses, without exception, are 1.4–1.8 times larger than the calculated masses, the ratio varying with  $\theta$ . For example, in the central section the ratio is  $\sim 1.4$  for  $H \parallel [\bar{1}10]$  and increases to 1.8 near fourfold axes. It is interesting that this ratio is approximately the same as for the small Fermi surface in the third zone.<sup>[1]</sup>

In conclusion the authors wish to thank Corresponding Member of the Ukrainian Academy of Sciences A. A. Galkin for his constant interest, as well as M. K. Gold'berg, A. I. Kononenko, É. M. Lifshitz, and V. D. Mil'man of the Department of Functional Analysis and Computational Mathematics of the Physico-technical Institute for devising an algorithm and programming the problem.

<sup>1</sup>Galkin, Naberezhnykh, and Mel'nik, FTT 5, 201 (1963), Soviet Phys.-Solid State 5, 145 (1963).

<sup>2</sup>Galkin, Naberezhnykh, and Mel'nik, Ukrainian Phys. J. 8, 81 (1963).

<sup>3</sup>W. A. Harrison, Phys. Rev. 118, 1182 and 1190 (1960).

<sup>4</sup>M. G. Priestley, Proc. of the 8th International Conf. on Low Temperature Physics, University of Toronto, Canada, 1960.

Translated by I. Emin